# High-resolution frequency-domain spectroscopy for water vapor with coherent and continuous terahertz wave

**Cunjun Ruan (阮存军)[1,2,*], Deyin Kong (孔德胤)[1], Jun Dai (戴 军)[1], Kanglong Chen (陈康龙)[1], Sujie Guo (郭素杰)[1], and Xiaojun Wu (吴晓君)[1]**

[1]*School of Electronic and Information Engineering, Beihang University, Beijing 100191, China*
[2]*Beijing Key Laboratory for Microwave Sensing and Security Applications, Beihang University, Beijing 100191, China*
**Corresponding author: ruancunjun@buaa.edu.cn*

Received January 16, 2019; accepted March 22, 2019; posted online June 6, 2019

High-resolution frequency-domain spectroscopy (FDS) is set up using a coherent and continuous wave terahertz (THz) emitter and receiver. THz waves are generated and detected by two photomixers with two distributed feedback (DFB) lasers. Atmospheric water vapor with different relative humidity is systematically investigated by the FDS. A high-frequency resolution of ~14 MHz is obtained with the help of Hilbert transformation, leading to a well resolved and distinct transmittance characterization of water vapor. Compared with conventional THz time-domain spectroscopy, the high-resolution continuous wave THz spectrometer is one of the most practical systems in gas-phase molecular sensing, identification, and monitoring.

*OCIS codes: 300.6495, 010.7340, 010.0280.*
*doi: 10.3788/COL201917.073001.*

Gas-phase molecules are strongly correlated to environmental pollution, drug detection, human breath analysis, and so on[1–5]. Therefore, qualitative and quantitative analyses of the gas-phase molecules are significantly important for many industrial applications.

Located between microwave and infrared frequency ranges, terahertz (THz, 0.1–10 THz) spectroscopy is one of the most important and powerful tools for gas molecules analysis[6]. By comparing the characteristic absorption signatures in THz gas-phase spectroscopy (0.03–3 THz), we can identify the composition of gas samples and monitor its concentration under suitable conditions[7]. THz spectroscopy systems used to monitor the gas-phase molecules are divided into time-domain spectrometers and continuous wave (CW) spectrometers[8–12]. Due to the existence of many sharp and crowded transitions of gases, THz spectrometers are not only required to have the characteristics of high-frequency resolution and high-detection sensitivity, but are also cost-effective, portable, stable, and reliable[13–15].

CW THz spectrometers are one of the most promising systems for practical applications, especially for gas-phase spectroscopy[16]. CW THz spectrometers based on photomixing not only have megahertz (MHz) frequency resolutions with the frequency range covering up to 3 THz, but also are very compact[17,18]. In particular, the recently developed CW THz coherent spectrometer [THz frequency-domain spectroscopy (FDS)] has become a powerful tool to study gas molecules and high $Q$-factor THz devices[19]. The frequency resolution of THz-FDS can be tuned by changing the optical path difference. By using a whispering gallery mode bubble resonator and employing Hilbert analysis, the frequency resolution can go to 4 MHz[19].

Compared with Fourier transform infrared spectroscopy (FTIR), the THz-FDS has a higher signal-to-noise ratio (SNR). It is very difficult for the FTIR to reach low frequencies (<1 THz) with very high SNR. The resolution of the most advanced FTIR Bruker IFS 125HR reaches 0.001 $cm^{-1}$ (30 MHz), and the spectral range is 20–1000 $cm^{-1}$ (0.6–30 THz), decided by the far-infrared synchrotron radiation[20]. This system takes up a lot of space in the laboratory, and the THz source of the system must work in an appropriate environment. Compared with THz time-domain spectroscopy (TDS), THz-FDS has the following advantages. (1) THz-FDS has a very high resolution, which is very useful for gas-phase molecules monitoring and remote sensing. In our system, if the Hilbert transformation is used to analyze the data, the resolution can reach the sampling frequency of 10 MHz, which is determined by the frequency step and frequency stability of the lasers. The frequency resolution of THz-TDS is determined by the time window of the scanning delay lines. Not only the reflection waves from the photoconductive antennas (PCAs) or the nonlinear crystal generators or detectors primarily limit the frequency resolution. Up to now, the best frequency resolution from THz-TDS can only go up to 0.9 GHz, while the THz-FDS can go up to ~4 MHz[19,21]. Therefore, for some specific molecular applications, high-resolution spectrometers are required. Also for some high-$Q$ devices like whispering gallery resonators[19], it has been demonstrated that only the THz-FDS can be applied to do this work. (2) THz-FDS does not need a femtosecond laser as a pump. It only needs two cost-effective distributed feedback (DFB) laser diodes, whose list price is less than half that of Ti:sapphire oscillators pumped THz-TDS. It has a great advantage in price. (3) The frequency resolution is easily adjusted based on the varied THz propagation path length or by altering the fiber lengths, which will be addressed in detail in the Letter. (4) This system has the

 

advantage of measuring only the interested part of the spectrum instead of measuring the whole range of the spectrum converted from the time-domain signal.

In our work, we demonstrate a high-frequency resolution of ~235 MHz THz-FDS and record the THz absorption spectroscopy of water vapor with different relative humidity (RH) in the atmosphere. The frequency resolution is increased to ~14 MHz by the Hilbert transformation method. Water vapor is the largest contributor to atmospheric attenuation for THz waves due to lots of vibrational and rotational states. It is important to investigate the THz properties of water vapor, especially for THz telecommunications and environment monitoring[22,23]. In comparison with THz-TDS, we verify that THz-FDS is even more powerful for gas-phase molecule spectroscopy applications.

In our measurements, we use a commercial TeraScan 780 system (Toptica) with two fiber-coupled GaAs log-spiral PCAs as the emitter and detector[24], respectively, as shown in Fig. 1. There are two DFB lasers with built-in optical isolators and fiber-optic beam combinations. The central wavelengths of the two lasers are 783 and 785 nm, respectively. The laser power per two-color fiber output is >40 mW. The typical frequency stability per laser is 20 MHz root mean square (RMS), 100 MHz peak-to-peak (p-p) at 5 h. The laser size and weight for two laser heads with each dimension are 80 mm × 80 mm × 270 mm and 2 kg, respectively. The CW spectrometer has a difference frequency tuning of 0.05–2.0 THz with a tuning speed up to 100 GHz/s. The absolute frequency accuracy is 2 GHz. The generated THz waves are with left-handed polarization with 2 μW at 0.1 THz and 0.3 μW at 0.5 THz. For the stability of the radiated THz waves, the system has a dynamic range (300 ms integration time) up to 80 dB at 100 GHz and 70 dB at 500 GHz, respectively. Four 90° off-axis parabolic mirrors are assembled to collimate and focus the emitted THz beam with high-precision position adjustment for coherent detection. This extends the interaction path and prepares for the future measurement of solid samples. The path length of THz-gas molecular interaction is calculated from the emission antenna to the detection antenna, and the whole THz beam path is ~846.4 mm, which includes four parabolic mirrors with focal lengths of 101.6 mm, two collimated radiation paths of 190 mm, and two THz silicon lenses with focal lengths of ~30 mm.

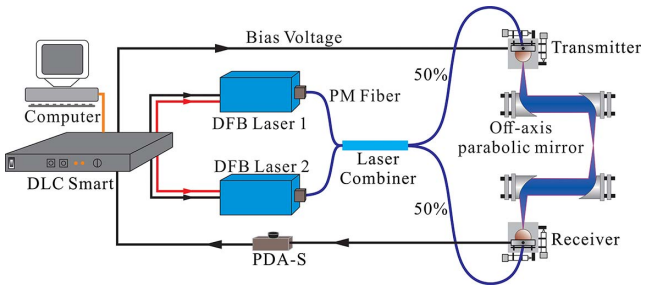


Fig. 1. Schematic of the THz-FDS.

The measured photocurrent at the detecting PCA not only depends on the amplitude of the generated THz electric field but also the phase difference between the THz waves and the detecting optical beat signal. Several methods can be employed to improve the spectral resolution. Hilbert transformation is a suitable method to acquire the envelope and instantaneous phase from such a signal in our system[19]. It can calculate the envelope and phase of all the points in the data, not just the extremes. By using Hilbert analysis[19], the resolution can be enhanced to several MHz, which is limited by the line-width and the stability of the two beating semiconductor lasers. The interaction length in our system is ~846.4 mm, and the conventional spectral resolution is ~235 MHz, as shown in the inset of Fig. 2.

Traditionally, the frequency resolution is calculated by the formula of $\Delta f = c/(2\Delta L)$, where $c$ is light speed, and $\Delta L$ is the difference between the optical paths, which is the difference of two optical paths from the laser combiner to the receiver, as shown in Fig. 1[18]. In this work, we use Hilbert transformation to analyze the data, and the spectral resolution can reach 14 MHz, which also is the frequency step in our measurement. More details for the determination of the frequency resolution can be found in Refs. [18,19].

To demonstrate the capability of the high-resolution CW THz spectroscopy, we measure the water vapor absorption at different RHs. There is no gas cell covering the THz propagation, and no dry nitrogen purging is used. The system is not sealed, and the environmental RH and temperature are measured by a commercial temperature hygrometer during the whole measurement process.

Figure 2 illustrates the acquired original data at RH 33.5% and the highlighted envelope of data. The oscillation in the envelope is caused by the Fabry–Pérot (FP) interference between the interfaces in the system, such

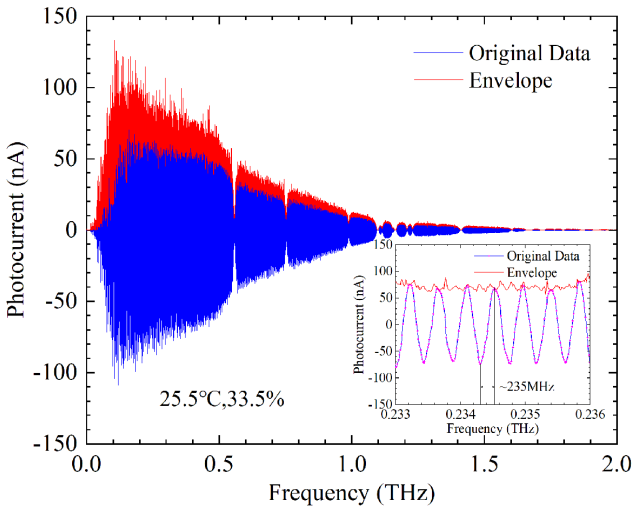


Fig. 2. Atmospheric water vapor transmittance signal measured by THz-FDS. The RH is 33.5%. The inset shows the obtained high resolution of 0.2 GHz.

as the surfaces between silicon lens and air, fibers and connectors.

In order to acquire a transmittance spectrum of some materials, a reference is needed, but getting rid of the water from the atmosphere is difficult for our open equipment. We try to manually normalize the data by curve fitting, as shown in Fig. 3. The original data is at the RH of 7.5%. The equation used for fitting is in Ref. [25] as

$$E_{\mathrm{THz0}} \propto I_{\mathrm{ph0}} = a_0 + \sum_{n=1}^{8} a_n \cos(nCf) + \sum_{n=1}^{8} b_n \sin(nCf), \tag{1}$$

where $a_n$, $b_n$, and $C$ are the unknown parameters, $f$ is the frequency, and $I_{\mathrm{ph0}}$ is the fitted photocurrent curve, which is in direct proportion to the THz electric field $E_{\mathrm{THz0}}$. Thus, the transmittance follows

$$T = \left(\frac{I_{\mathrm{ph}}}{I_{\mathrm{ph0}}}\right)^2, \tag{2}$$

where $I_{\mathrm{ph}}$ is the measured photocurrent. The results are shown in Fig. 4. The information system spectroscopy of atmospheric gases (SPECTRA) offers a useful tool for the simulation of mixed gases[26]. The simulation results in Fig. 4 well match the measured data. The difference may be caused by errors in the measurement of temperature and humidity, and the deviation in frequency is due to the instability of the lasers. As shown in Fig. 4, there are ~16 absorption peaks that can be identified, which also agrees very well with the results measured on THz-TDS, which will be discussed in the following. The absorption lines located at ~0.558, ~0.753, and ~0.989 THz are obviously resolved. The absorption bands located around 1.6 THz are also observed, but not so well resolved due to low SNR and extremely strong absorption. This noise can be reduced by a long integration time. In Fig. 4, the peaks of the original transmittance at ~0.989 THz almost cannot be identified, but the smoothed curve in Fig. 4 shows a clear figure of this peak. The narrow peaks at ~1.52 and ~1.98 THz are caused by the noise. At high frequency, this error happens more frequently. Therefore, our system is suitable for p-p of ~230 Pa (1.7 Torr) or even under 200 Pa.

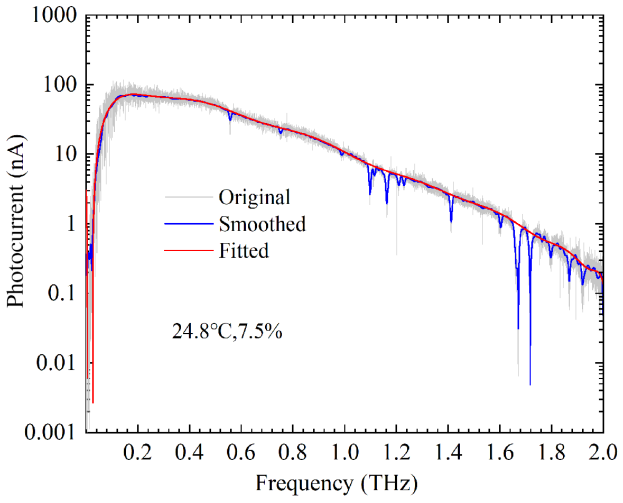


Fig. 3. The gray curve is the envelope of the atmospheric water vapor transmittance signal, the blue one is the smoothed curve, and the red one is the fitted curve regardless of the absorption peaks. The RH is 7.5%, and the temperature is 24.8°C.

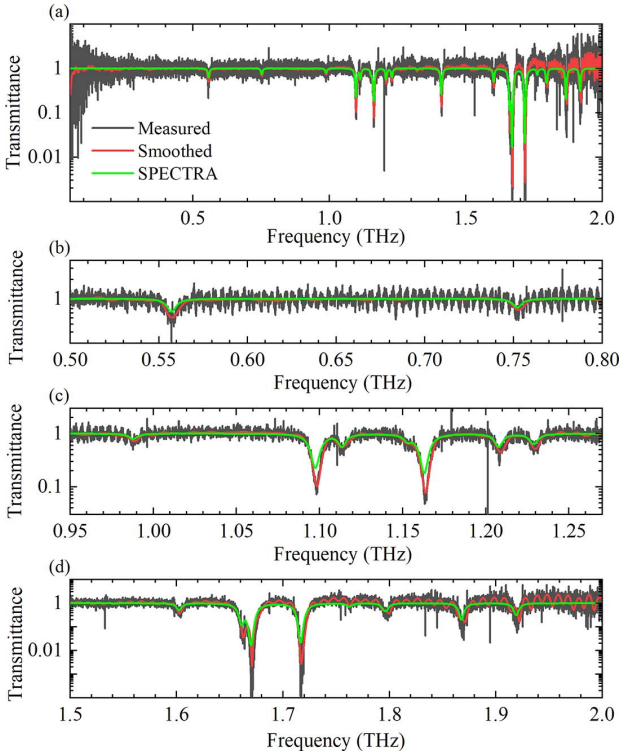


Fig. 4. The gray curves are the transmittance spectra of the atmospheric water vapor, the red curves are the smoothed results, and the green curves are the simulated results of SPECTRA. (a) The whole spectrum from 0.05 to 2 THz. (b), (c), and (d) Parts of the spectrum. The RH is 7.5%, and the temperature is 24.8°C (234.9 Pa).

In order to compare the THz spectroscopy of water vapor measured with both time-domain and frequency-domain spectrometers, a conventional home-made THz time-domain spectrometer is employed to measure the absorption of water vapor with different RHs. A low-temperature grown GaAs PCA is used to generate THz pulses, and a ZnTe crystal is applied for electro-optic sampling measurement. The emitted THz frequency range is 0.2–2.5 THz with a high dynamic range of >5000. The scanning time window is limited by the THz reflection from the GaAs PCA and the ZnTe detector. Therefore, the time window is 40 ps with a corresponding frequency resolution of 33 GHz.

In order to verify the sensitivity of THz-FDS, we measure the atmospheric water vapor absorption of $7.5\% \pm 0.6\%$, $12.0\% \pm 0.9\%$, $26.0\% \pm 0.8\%$, $33.5\% \pm 0.7\%$, and $40.2\% \pm 1.6\%$. The temperatures of them are $24.8°C \pm 0.2°C$, $25.0\% \pm 0.4°C$, $25.0°C \pm 0.3°C$,

**Table 1.** Partial Pressure

| Temperature (°C) | Relative Humidity (%) | Partial Pressure (Pa) |
|---|---|---|
| 24.8 | 7.5 | 234.9 |
| 25.0 | 12.0 | 380.4 |
| 25.0 | 26.0 | 824.2 |
| 25.5 | 33.5 | 1094.0 |
| 26.5 | 40.2 | 1392.8 |

25.5°C ± 0.2°C, and 26.5°C ± 0.2°C. The calculated p-p is shown in Table 1, and the results are shown in Fig. 5. Due to crowded absorption lines and strong absorption coefficients at higher frequencies, it is very difficult to obtain obviously resolved water vapor absorption lines for the frequencies. The other reason is the output power of the THz emitter at higher frequencies is relatively low, less than 0.1 μW. The water vapor absorption signatures reduce when the RH decreases. For the three lower frequencies of ∼0.558, ∼0.753, and ∼0.989 THz, they can hardly be detected when the RH is ∼7.5%. Figure 5(b) exhibits the enlarged absorption lines at 0.558 THz measured for RHs of 40.2%, 33.5%, 26%, 12%, and 7.5%, respectively. The frequency difference between the simulated results and the measured ones may be caused by the influence of water clusters[9]. The water clusters in high humidity may have special properties.

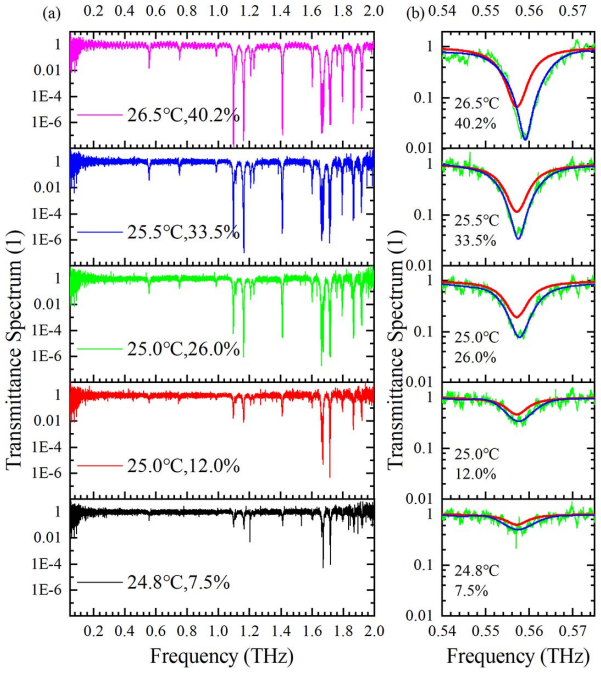


Fig. 5. (a) Water vapor transmittance spectra measured by THz-FDS at RHs of 40.2%, 33.5%, 26%, 12%, and 7.5%, respectively. (b) The enlarged view of the transmittance spectra at 0.558 THz for different RHs. Green, measured results; red, simulated results; blue, smoothed result.

When the RH decreases, the interference signals from the standing waves of the system caused by the FP effect, for example, from the interface between the air and the silicon lens, turn out to be dominant. This noise limits the system's ability for trace substance. Up to now, there is no good way to eliminate these phenomena. In our case, we try to remove the oscillations by converting the spectrum to a calculated time-domain signal, where the oscillations and main signal can be distinguished by the intensity. This method is like Fourier self-deconvolution (FSD)[27]. The differences are that FSD is suitable for the absorption spectroscopy, but, in our work, the targeted data is the original data, which contains the transmission coefficient spectrum. The results are shown in Figs. 3, 4, and 5(b).

During our experiments, we find that the THz-FDS is very sensitive to the RH. Therefore, it may become a highly sensitive remote monitoring system for water vapor, especially in some specific conditions, such as vacuum chambers, high altitudes, and outer space water vapor detection. For the fact that the temperature difference of the five data is small, we can get the peaks' transmittance changed with RH at 0.558, 0.753, and 0.989 THz.

In Fig. 6, for the three frequencies, the transmittance decreases with RH and frequency. The error at RH 7.5% is caused by the low SNR, which is due to FP interference. RH cannot directly represent the amount of water vapor, but, in our results, the deviation of temperature is low, so the RH is approximately in direct proportion to the p-p. In our system, 0.558 THz is near the peak intensity of the source output energy, so the signal is strong, and the absorption of water is large enough for identification under the effect of FP interference. It means that the absorption peak at 0.558 THz is more appropriate for remote sensing of atmospheric water vapor in this system.

In order to verify the absorption lines of water vapor and compare the capability between pulsed THz sources and CW THz sources, a conventional THz-TDS is applied

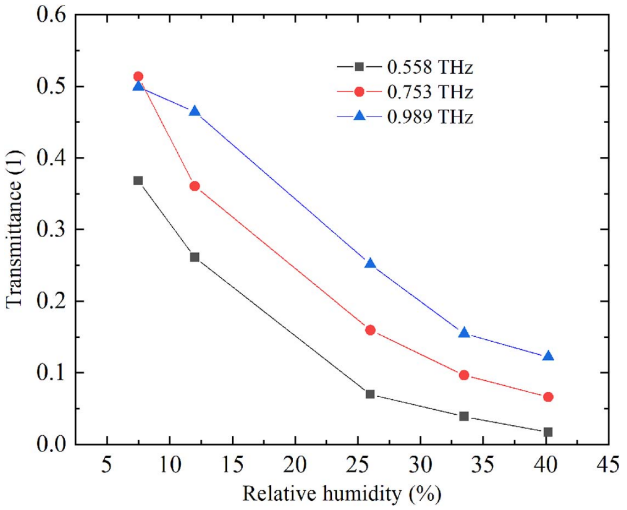


Fig. 6. Transmittance at 0.558, 0.753, and 0.989 THz for different RHs of 40.2%, 33.5%, 26%, 12%, and 7.5%, respectively.

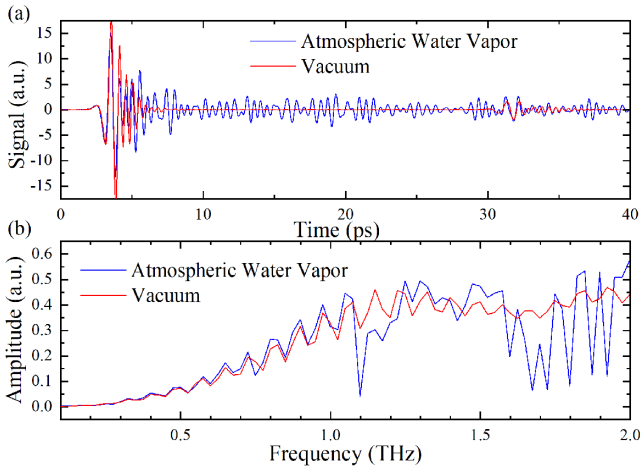


Fig. 7. (a) Measured THz temporal waveform of the atmospheric water vapor (blue curve) and vacuum (red curve), and (b) the corresponding Fourier transform spectrum of the two kinds of environments, respectively.

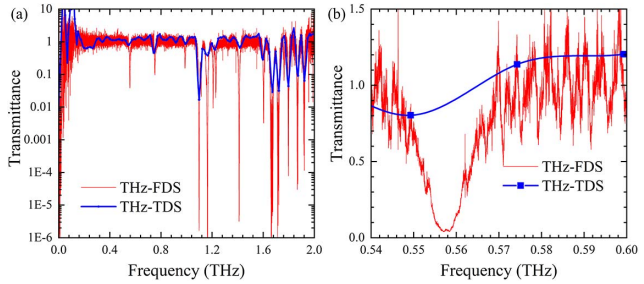


Fig. 8. (a) Merged spectra of atmospheric water vapor measured by THz-TDS and THz-FDS. (b) Comparison of the zoom in graph for the absorption line at 0.558 THz.

to measure the water vapor. Figure 7 provides the typical THz temporal waveforms and their corresponding spectrum. For a better resolution, we choose the longest time, where the reflection signal can also be measured, as shown in the temporal waveform of the vacuum in Fig. 7(a). Due to limited resolution, the lower-frequency absorption lines at 0.558, 0.753, and 0.989 THz can be observed but not well resolved. Further comparison between THz-FDS and THz-TDS is summarized in Fig. 8. The spectrum of the THz-FDS is measured at the RH of 33.5%. We can see in Fig. 8(a) that almost all the absorption lines can be measured in the two systems. However, the THz-FDS has obviously much higher frequency resolution, resulting in more points and accurate measurements, referring to Fig. 8(b). This is very important for gas-phase spectroscopy, in which high-resolution is needed for material identification.

This work was supported by the National Natural Science Foundation of China (Nos. 61831001 and 61222110), the High-Level Talent Introduction Project of Beihang University (No. ZG216S1878), and the Youth-Top-Talent Support Project of Beihang University (No. ZG226S1821).

## References

1. P. F.-X. Neumaier, K. Schmalz, J. Borngräber, R. Wylde, and H.-W. Hübers, The Analyst **140**, 213 (2015).
2. D. Bigourd, A. Cuisset, F. Hindle, S. Matton, R. Bocquet, G. Mouret, F. Cazier, D. Dewaele, and H. Nouali, Appl. Phys. B Lasers Opt. **86**, 579 (2007).
3. K. P. V. Rivera, A. M. Gallego, J. M. Hernández, A. Monroy-Guzmán, Y. Mares-Gutiérrez, J. A. Christen, L. G. Ruiz-Suárez, S. Alavez, and A. M. Juárez, AIP Conf. Proc. **1747**, 030001 (2016).
4. H. Cai, D. Wang, and J. Shen, Sci. China Phys. Mech. Astron. **56**, 685 (2013).
5. H. Zhang, Z. Zhang, X. Zhao, X. Zhang, T. Zhang, C. Cao, and Y. Yu, Chin. Opt. Lett. **16**, 103001 (2018).
6. M. van Exter, C. Fattinger, and D. Grischkowsky, Opt. Lett. **14**, 1128 (1989).
7. J. S. Melinger, Y. Yang, M. Mandehgar, and D. Grischkowsky, Opt. Express **20**, 6788 (2012).
8. A. S. Pine, R. D. Suenram, E. R. Brown, and K. A. McIntosh, J. Mol. Spectrosc. **175**, 37 (1996).
9. Y. D. Wu, T. Zhou, Z. W. Yao, and J. C. Cao, J. Appl. Spectrosc. **83**, 362 (2016).
10. Y. Yang, A. Shutler, and D. Grischkowsky, Opt. Express **19**, 8830 (2011).
11. Y. Yang, M. Mandehgar, and D. Grischkowsky, Opt. Express **20**, 26208 (2012).
12. X. Wu, S. Chai, J. Ma, B. Zhang, C. Xia, Z. Fang, D. Kong, J. Wang, H. Liu, C. Zhu, X. Wang, C. Ruan, and Y. Li, Chin. Opt. Lett. **16**, 041901 (2018).
13. F. S. Vieira, F. C. Cruz, D. F. Plusquellic, and S. A. Diddams, Opt. Express **24**, 30100 (2016).
14. Z. Mihoubi, K. G. Wilcox, S. Elsmere, A. Quarterman, R. Rungsawang, I. Farrer, H. E. Beere, D. A. Ritchie, A. Tropper, and V. Apostolopoulos, Opt. Lett. **33**, 2125 (2008).
15. G. Mouret, F. Hindle, A. Cuisset, C. Yang, R. Bocquet, M. Lours, and D. Rovera, Opt. Express **17**, 22031 (2009).
16. W. Shi and Y. J. Ding, Laser Phys. Lett. **1**, 560 (2004).
17. A. J. Deninger, A. Roggenbuck, S. Schindler, and S. Preu, J. Infrared Millim. Terahertz Waves **36**, 269 (2014).
18. A. Roggenbuck, H. Schmitz, A. Deninger, I. C. Mayorga, J. Hemberger, R. Güsten, and M. Grüninger, New J. Phys. **12**, 043017 (2010).
19. D. W. Vogt and R. Leonhardt, Opt. Express **25**, 16860 (2017).
20. G. L. Carr, R. J. Smith, L. Mihaly, H. Zhang, D. H. Reitze, and D. B. Tanner, Infrared Phys. Technol. **51**, 404 (2008).
21. T. Seta, H. Hoshina, Y. Kasai, I. Hosako, C. Otani, S. Loßow, J. Urban, M. Ekström, P. Eriksson, and D. Murtagh, J. Quant. Spectrosc. Radiat. Transf. **109**, 144 (2008).
22. Y. Yang, M. Mandehgar, and D. Grischkowsky, J. Infrared Millim. Terahertz Waves **36**, 97 (2015).
23. C. Lin, I. Ho, and X. C. Zhang, Chin. Opt. Lett. **10**, 043001 (2012).
24. I. Cámara Mayorga, E. A. Michael, A. Schmitz, P. van der Wal, R. Güsten, K. Maier, and A. Dewald, Appl. Phys. Lett. **91**, 031107 (2007).
25. G. P. Tolstov, *Fourier Series* (Courier Corporation, 2012).
26. C. N. Mikhailenko, Y. L. Babikov, and V. F. Golovko, Atmos. Ocean. Opt. **18**, 685 (2005).
27. J. K. Kauppinen, D. J. Moffatt, H. H. Mantsch, and D. G. Cameron, Appl. Spectrosc. **35**, 271 (1981).